Gas adsorption on single-wall carbon nanotube bundles and charcoal samples

Y. H. Kahng, R. B. Hallock, and E. Dujardin

Phys. Rev. B **83**, 115434 — Published 16 March 2011

DOI: 10.1103/PhysRevB.83.115434

Gas adsorption to Single-Wall Carbon Nanotube Bundles and Charcoal Samples

Y. H. Kahng,[1,*] R. B. Hallock,[1,†] and E. Dujardin[2]

[1]*Laboratory for Low Temperature Physics, Department of Physics, University of Massachusetts, Amherst, MA 01003, USA*

[2]*NanoSciences Group, CEMES / CNRS UPR 8011, Toulouse, France*

(Dated: January 5, 2011)

We have studied the adsorption properties of ^{4}He on single-wall carbon nanotube (SWNT) bundles and activated carbon (charcoal) samples using a temperature-programmed desorption (TPD) technique. The ^{4}He binding energy, the dose temperature dependence of adsorption, and the competitive adsorption of binary mixture gases among ^{4}He, ^{3}He, H_2, and Xe were measured. The ^{4}He binding energy on SWNT was as high as 910 K at $\sim 1 \times 10^{17}$ atom/mg coverage, decreased as the coverage increased and agrees with the previously reported energy values where the coverages overlap. On charcoal the ^{4}He binding energy was constant at 403±11 K. ^{4}He adsorption showed an activated adsorption behavior when ^{4}He was dosed below ∼30 K with activation energy ∼20 K to some sites of the SWNT bundles. We argue that these sites are interstitial channel (IC) sites, and the activated adsorption was the reason why some of the previously reported gas adsorption studies where ^{4}He was dosed at low temperature could not detect IC adsorption. On charcoal ^{4}He did not show activated adsorption behavior when dosed at ∼15 K. Mixture gas adsorption measurements on SWNT samples showed the relative binding strengths were $^3\text{He} < {}^4\text{He} < H_2 < \text{Xe}$. Results showing $^3\text{He} < {}^4\text{He}$ coincide with the predictions of quantum sieving on SWNT bundles. When ^{4}He was dosed at 275 K and H_2 was dosed at 19 K, ^{4}He adsorption was stable against H_2, which indicates limited access of H_2 at low temperature to some of the sites where ^{4}He pre-adsorbed. Again we argue that the likely candidate for such sites are IC sites on SWNT bundles.

PACS numbers: 68.35.Md,68.43.Fg,81.07.De

I. INTRODUCTION

Since their discovery, Carbon Nanotubes had considerable interest due to their exciting new physical and chemical properties[1,2]. Single-Wall Carbon Nanotubes (SWNT)[3] have been studied with various points of focus, *e.g.* their possible use as a hydrogen storage medium[4,5], molecular sieves to separate isotopes and ions[6–8], and a substrate for one-dimensional (1D) adsorbate studies[9–30].

Our study is focused on SWNT bundles as a 1D substrate using gas adsorption. There are expected to be three different adsorption binding sites that show 1D characteristics, the interstitial channels (IC) in the bundle where three tubes meet, the inner diameter (ID) of individual nanotubes, and the outer grooves (OG) on the surface of the bundles where two nanotubes meet. For our closed-end SWNT bundles, ID sites are not available for gas adsorption. Therefore we will not mention ID sites further below.

While many theoretical studies have predicted rich physics in the adsorbate gas system on various adsorption sites[9–11,13,17], it is not conclusively determined experimentally where the gas molecules adsorb in SWNT bundles; *e.g.*, small atom or molecule access to IC sites has not been confirmed experimentally[19,21] despite theoretical predictions[10,11]. And the relative binding strength of these various potential binding sites has not been established experimentally for various adsobates[15,16,18–20,23–29].

This work addresses the binding of ^{4}He to SWNT bundles using a temperature-programmed desorption (TPD) technique. The ^{4}He binding energy on SWNT samples was measured and compared with the ^{4}He binding energy on a charcoal sample. Temperature dependent adsorption of ^{4}He and H_2 was measured on SWNT bundles and a charcoal sample. Relative binding strengths among ^{3}He, ^{4}He, H_2, and Xe on SWNT bundles are reported.

II. THEORETICAL PREDICTIONS

Stan *et al.*[10] predicted the binding energies of simple gas species such as helium, hydrogen, and xenon to the various sites on SWNT bundles. They also indicated that hydrogen, which has a higher binding energy than helium on general surfaces, will have a smaller binding energy on IC sites due to size effects. A subset of their results for helium, hydrogen, and xenon is shown in Table I. Work by Calbi *et al.*[11] included various interactions among the adsorbed species on the IC sites and interactions between adsorbates and the nanotubes that make up the bundles. Such interactions are predicted to have substantial effects, including, for example, the prediction that hydrogen will be more strongly bound to the IC than will helium due to weak dilation of the SWNT bundle. The predicted binding energies for helium and hydrogen in the ground state at optimal density for the dilated SWNT bundle[11] are also shown in Table I. However, the experimental observations by Bienfait *et al.*[31] have set the extent of the dilation in SWNT bundles below 0.5%.

TABLE I: Single molecule ground state energies (in Kelvin) predicted for helium, hydrogen, and xenon located at two possible 1D sites (IC and OG) on SWNT bundles and on a graphite surface (GR)[10]. Also shown are the optimal-density, ground state binding energy values for helium and hydrogen on the IC sites for dilated SWNT bundles (D)[11].

Sites	^{4}He	H_2	Xe[a]	^{4}He (D)	H_2 (D)
IC	-386	-292	15054	-381	-481
OG	-270	-618	-2580	-	-
GR	-166	-383	-1573	-	-

[a]Note that positive energy on IC indicates repulsion.

III. EXPERIMENTAL

A. Samples

We have used two types of samples in our gas adsorption work: single-wall carbon nanotube (SWNT) bundles and activated carbon (charcoal). For the SWNT samples, we have observed that when SWNT samples contacted room air, the ^{4}He adsorption capacity of the sample decreases significantly[29], an observation that may be relevant to many previous studies made by others. In this study, we kept all of our samples in vacuum-sealed quartz vials exposing them to the adsorbate gas by breaking the vial by a mechanical feed-through in the protected environment of the sample cell. More details about this procedure have been reported elsewhere[32].

We examined the effect of vacuum-pumping the SWNT sample at ∼500°C for one hour (vacuum-baking) on the ^{4}He adsorption capacities. After samples had contacted room-air, vacuum-baking increased the ^{4}He adsorption capacity back to the level of the original sample[53]. All of the samples used in our study were vacuum-baked either right after the sample synthesis and purification or after some gas adsorption experiments and exposure to room air. To be consistent, we have maintained the same sample preparation protocol on the charcoal sample as well.

Our SWNT samples were prepared using a laser vaporization method[33]. After production, the sample was purified in boiling Nitric acid[34] and baked at 500 °C under vacuum ($\sim 5 \times 10^{-6}$ torr) for one hour before being sealed in a glass vial. The SWNT sample was kept in the vial under vacuum before the measurements. Fig. 1 is a transmission electron microscope (TEM) image of a section of one of the samples used in this experiment. Electron microscopy and spectroscopic studies done on the sample have confirmed that our sample is quite pure, but none-the-less contains some impurities such as catalysts and carbonaceous materials. We estimate the purity of our SWNT sample to be ∼95%. Our sample was not processed to open the end caps[35], so most of the end caps are expected to be closed. With intact end caps, there are two kinds of sites in the bundle that are expected to show high binding energies: outer grooves (OG) and interstitial channels (IC). However, if some of the end caps were damaged during the purification process, then the inner tube sites could have affected our adsorption data especially in the low coverage regime.

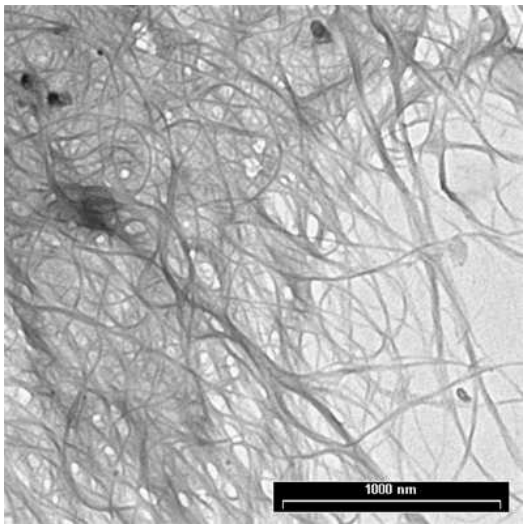

FIG. 1: A TEM image of part of one of the SWNT samples used in these experiments. Tangled SWNT bundles are shown. The scale bar is one μm.

Four SWNT samples were used in this study. The masses of the samples were, SWNT1 = 2.7 mg, SWNT1-1 = 2.1 mg, SWNT1-2 = 0.37 mg, and SWNT2 = 1.5 mg. The uncertainty of the sample mass was about 20% for all the samples. Such high uncertainty orignated from difficulty in extracting the SWNT samples out of broken quartz pieces after the adsorption measurements. The SWNT1 and SWNT2 samples were the samples that were freshly prepared after purification and kept in vials, and the SWNT1-1 and SWNT1-2 samples were prepared again by vacuum-baking after the gas adsorption studies.

We used charcoal for a comparison study of the adsorption to SWNT bundles. Our sample was obtained from the Low Temperature Laboratory at the University of Florida at Gainesville. Originally the sample was purchased from Norit Americas, Inc. We examined the charcoal sample with X-ray Photoelectron Spectroscopy (XPS) and confirmed that our sample mostly consisted of carbon. The charcoal sample consisted of ∼1 mm size particles. A scanning electron microscope (SEM) study revealed that the surface of each particle had ∼1 micron size pores. A section of a surface of a charcoal particle is shown in Fig. 2. We used one charcoal sample, which had a mass of 4.2±0.4 mg.

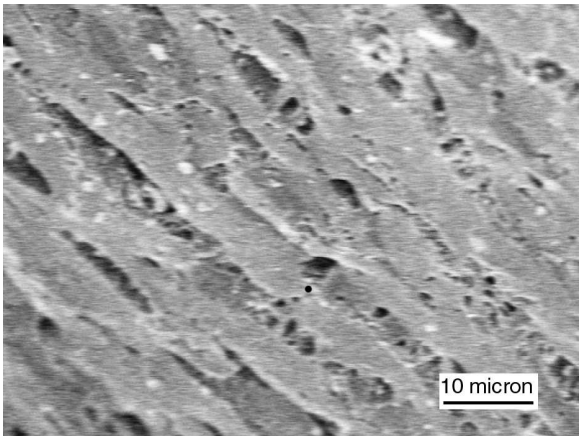

FIG. 2: A SEM image of part of the charcoal sample used in our experiments. A section of the charcoal grain surface is shown, showing ∼1 micron wide pores which also had substructures. The scale bar is ten μm.

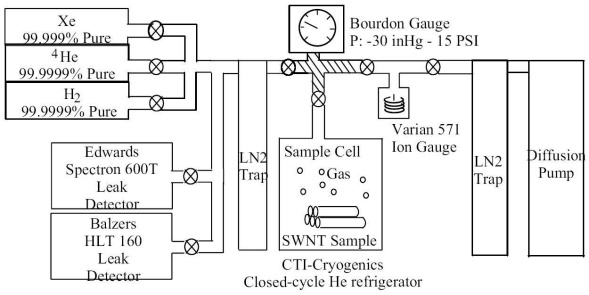

FIG. 3: A schematic of the apparatus. Three different gases (^{4}He, H_2, and Xe or ^{3}He) could be simultaneously attached and studied. The gas-in line and pump-out line had a liquid nitrogen (LN2) trap. A bourdon pressure gauge was used to measure the gas dosage pressure to the sample cell. The volume used to calculate the gas dosage is shaded in the schematic. The sample cell was attached to a closed-cycle helium refrigerator inside the vacuum can. One (two) mass spectrometer equipped leak detector(s) was (were) used when we measured (co)desorption from the sample.

B. Apparatus and Experimental Procedure

A Temperature-Programmed Desorption (TPD) technique was used in this experiment[36]. Fig. 3 is a schematic diagram of the experimental apparatus. The background pressure of our system was $\sim 10^{-7}$ torr. Although we will be more specific later, the general protocol used for this work was as follows. The glass vial that contained the SWNT sample was broken at a pressure of 760 Torr ^{4}He inside the sample cell (SC) at ∼300 K using a mechanical feed-through. After the sample was exposed to ^{4}He gas, the temperature of the SC was lowered to a desired temperature (T_{low}), following which the SC was evacuated for about 10 hours using a diffusion pump (T_{low}-pump-out). The temperature lowering was done at the maximum speed of the refrigerator which typically took about three hours.After pumping, the SC temperature was warmed up at a rate of ∼0.02 K/sec while monitoring the gas desorption signals with calibrated mass spectrometer leak detectors. When the SC temperature reached about 190 K, desorption monitoring was stopped and the SC was pumped with a diffusion pump while further warming up to ∼275 K in order to further clean the sample. At 275 K, the SC was recharged with the studied gas at approximately 300 Torr (high-T dose, the molar quantity of the dosed gas was controlled to be constant.), and the protocol was repeated.

For some experiments, the gas dose temperature (T_{dose}) was changed to a low temperature (low-T dose). When a low temperature dose was done, the SC was cooled down from 275 K to a preset T_{dose} then gas was dosed to the SC for a certain amount of time (dose-time) then the SC temperature was adjusted to a preset T_{low} then the T_{low}-pump-out was done and the rest of the procedures (warm up while monitoring the desorption signal) mentioned above were followed.

IV. MEASUREMENT RESULTS AND DISCUSSION

The temperature-programmed desorption (TPD) experiments on the SWNT bundle and charcoal samples were performed along the lines described above. ^{4}He binding energies, the temperature dependence of ^{4}He and H_2 adsorption, competitive adsorption of binary mixtures among ^{3}He, ^{4}He, H_2, and Xe are next presented in turn and in detail.

A. ^{4}He Binding Energies on Single-wall Carbon Nanotube Bundles and on Charcoal

Two types of analysis techniques have been used to obtain the binding energy from the TPD data. First, we used the two-state binding model[37] to analyze the data to obtain the binding energy, which fit well to the charcoal sample data but did not fit well to the SWNT sample data. Second, we used the desorption rate isotherm analysis technique[38] to analyze the SWNT sample data and obtained the coverage-dependent ^{4}He binding energy. On the charcoal sample, the ^{4}He binding energy was coverage-independent at 403±11 K which agrees with a previously reported value by Jäckel and Fietzke[39]. On the SWNT sample, the ^{4}He binding energy was coverage-dependent and agrees with O.E. Vilches group's measurements[25] where the coverage overlaps, however our values increased further at the lower coverages, reaching as high as 910 K. This high binding energy value might indicate that there may be higher binding energy sites other than the previously predicted ones. For example, recent theoretical predictions by Calbi *et al.* predicted that high binding energy sites exist at the entrance to IC sites[12].

Fig. 4 shows the TPD spectra of ^{4}He from the char-

coal and from the SWNT1-1 sample. The ^{4}He desorption curves from charcoal changed their size more rapidly as T_{low} increased compared to curves from the SWNT sample. And among the charcoal curves, the bigger desorption curves always envelope the smaller curves. However, among the SWNT curves, some of the smaller curves were not enveloped by the bigger curves. The charcoal behavior was consistent with ^{4}He desorption from constant binding energy sites, and the SWNT curves behavior suggests the presence of deeper binding energy sites and T_{low}-dependant distribution of adsorbates on these sites, for which the physics is not clearly understood.

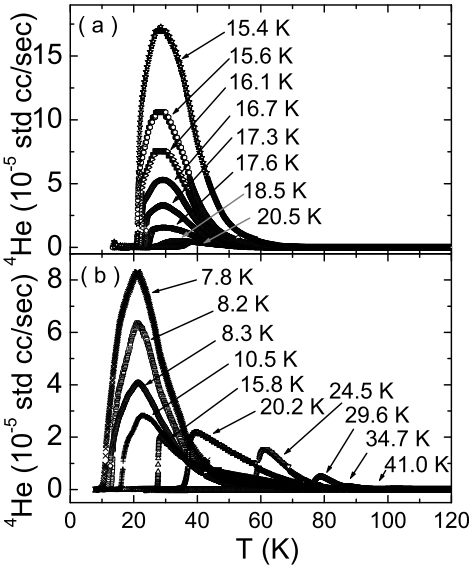

FIG. 4: ^{4}He desorption curve comparison between charcoal and SWNT samples. (a) shows charcoal sample curves and (b) shows SWNT1-1 sample curves. T_{low} values are indicated in the graphs. Here the signals have not been corrected for the different masses of the two samples.

After obtaining the TPD spectra, we integrated the ^{4}He desorption curves in order to obtain the initial ^{4}He coverage *vs.* T_{low} values as shown in Fig. 5. The charcoal and SWNT1-1 sample data are both plotted in the figure. The ^{4}He adsorption amount decreased more rapidly on the charcoal sample as the T_{low} value increased.

We applied the two state binding model[37] to the ^{4}He coverage *vs.* T_{low} data from both samples (Fig. 5 and Fig. 6). In the two-state binding model, the probability of binding (p_b) is given as, $p_b = [exp((E_b - \mu)/k_bT)+1]^{-1}$, where E_b is the binding energy, k_b is the Boltzmann constant, T is the absolute temperature, and μ is the chemical potential in equilibrium with the ideal gas reservoir. The number of adsorbed atoms (N_A) is given as $N_A = p_b \times x$ where x is the number of (monolayer) binding sites on the surface. Setting E_b (binding energy) and x (number of binding sites) as fitting variables, we obtained a best fit using a random downhill algorithm[40]. The data from the charcoal sample fitted well to this model (Fig. 5). The obtained ^{4}He binding energy of 403 ± 11 K was consistent with a value of 400 ± 32 K previously reported by Jäckel and Fietzke[39].

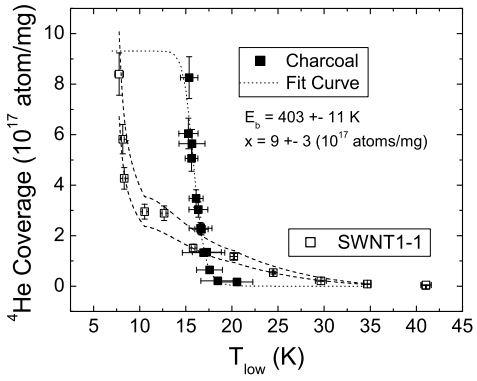

FIG. 5: ^{4}He adsorption capacity comparison between the charcoal and the SWNT1-1 sample per mg of sample. ^{4}He adsorbed to the charcoal more than to SWNT1-1 when the T_{low} value was below ∼17 K, but at higher T_{low} values, it was the other way around. The decrease in ^{4}He adsorption amount with increasing T_{low} values for the charcoal sample was more abrupt than for the SWNT sample. Two-state binding model fit to the ^{4}He adsorption on charcoal data is also shown by the dotted line. The fitted parameters are indicated. There is about 20% additional uncertainty which could shift the SWNT1-1 data set relative to the Charcoal data set as the dashed lines mark the range of shifts. This additional uncertainty originated from the sample mass uncertainty.

On the contrary, for the SWNT data, a two-state binding model fit with one curve did not produce a good fit, which is consistent with our previous report[27]. Fig. 6 shows the fitting results. To cover the whole data range, three curves with different fitting parameters were needed. This result suggests that on the SWNT sample, the ^{4}He binding energy is coverage-dependent in the range of ∼200-600 K.

To obtain the coverage-dependent ^{4}He binding energy on the SWNT sample more accurately, we tried a different approach called the desorption rate isotherm analysis[38]. In order to implement this analysis on the ^{4}He desorption data, several desorption spectra with different initial coverages were needed. All the desorption curves should have an identical warm-up profile. To obtain such data, we have added a T_{min}-cool-down procedure (which cools down the sample cell temperature to the minimum temperature of the refrigerator) before the warming-up procedure and after the T_{low}-pump-out procedure.

After changing the experimental procedure we observed a change among the desorption curves. Comparison can be seen on Figs. 4b and 7 of the data taken with and without the T_{min}-cool-down procedure. Without the T_{min}-cool-down procedure we observed that

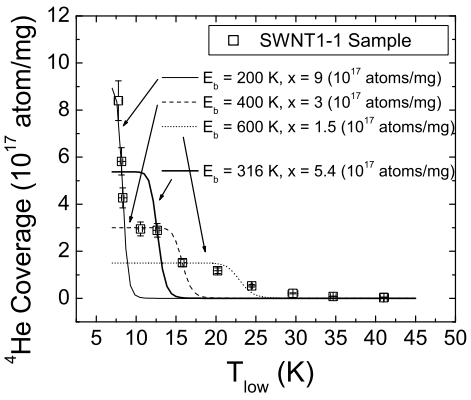

FIG. 6: Two-state binding model fits to the ^{4}He adsorption on SWNT data. Fitting with one curve (thick solid line) did not produce a good fit. Combination of three curves (thin lines) with different fitting parameters were needed to fit the whole trend of the data. The fitting results are indicated on the plot. For three combination fitting, the number of data points that support each fitted curve is small, therefore the fit results should only be taken as very approximate.

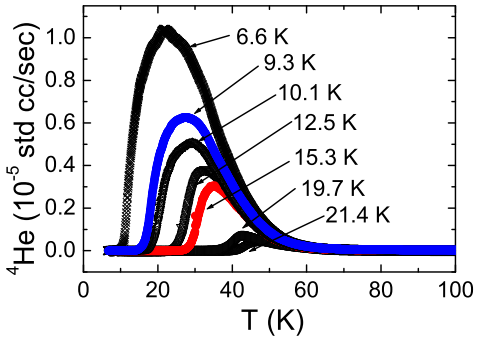

FIG. 7: (color online) ^{4}He desorption curves from SWNT1-2 sample with T_{min}-cool-down procedure. All the smaller desorption curves are contained within bigger desorption curves.

the smaller desorption curves (which were pumped at a higher T_{low} value) were not always contained within the bigger desorption curves (Fig. 4b). With the T_{min}-cool-down procedure the smaller curves were all contained within the bigger curves (Fig. 7).

In both sets of curves, the peak temperature shifted toward higher temperature as T_{low} became higher. This means that the smaller curves behaved as if the desorbing atoms were from the higher binding energy sites than the ones from the bigger curves. This observation supports the above conclusion that on the SWNT sample the binding energy of ^{4}He is highly coverage-dependent[25].

As we mentioned above, the reason why some of the smaller curves were not contained within the bigger curves in Fig. 4b is not clearly understood. It may be partly due to the difference in the warming-up temperature profile. There was typically an abrupt temperature increase at the beginning of the warming-up procedure before a linear-increase stabilized. And the curves with higher T_{low} values experienced such temperature increase at the proceeding edge of the desorption peak shifting the peak temperature to higher values. All the curves in Fig. 7 had a similar temperature warming-up profile and therefore the effect of different warming-up temperature profile is not present in these data.

We obtained two sets of ^{4}He desorption curves on two samples (SWNT1-2 and SWNT2). The ^{4}He adsorption amount *vs.* T_{low} data of these two samples were similar in trend and size to the data shown in Fig. 6.

The desorption rate isotherm analysis consists of several steps. The first step is to obtain the desorption rates at a constant ^{4}He coverage from different desorption curves with various initial coverages (Fig. 7). The second step is to plot the desorption rate *vs.* reciprocal temperature obtained from step 1 at different constant coverages as shown in Fig. 8 for the SWNT1-2 sample data. The SWNT2 sample data was similar. In this plot, the slope of a line obtained at a constant coverage yields the activation energy for desorption (E_d) at that coverage.

We observed ranges of data showing two distinct slopes. In the high desorption rate regime (where the desorption curves are near their peaks) the slopes were smaller compared to the slopes in the low desorption rate regime.

It is interesting to note that Muris *et al.*[16] have reported such a two-slope behavior in their logarithmic pressure (P) *vs.* reciprocal temperature (T) data of CH_4 isosteric heat measured on SWNT bundles in the 78 and 100 K temperature range. They attributed this changing behavior in slope on the log P *vs.* 1/T graph as evidence of an adsorbate phase transition. However, it was argued later that there could have been some experimental error on these results[41].

We obtained two slopes separately from the two regimes and plotted them together in Fig. 9. The activation energy of desorption values obtained from the low desorption rate regime (squares) were bigger ranging from 230 K to 910 K and were highly coverage-dependent. The energy value decreased as the coverage increased. On the other hand the activation energies obtained from the high desorption rate regime (circles) were smaller at around 100 K and did not show such strong coverage dependence.

The low activation energy values from the high desorption rate regime are similar to the ^{4}He binding energy on graphite (166 K). This seems to suggest that ^{4}He desorbed from the surface of the nanotubes (which has similar shape as graphite) at the outer surface of bundles during strong desorption. This may indicate that ^{4}He adsorbates from the higher binding energy sites can first migrate to the nanotube surface sites where the binding energy is around 100 K before the desorption when the

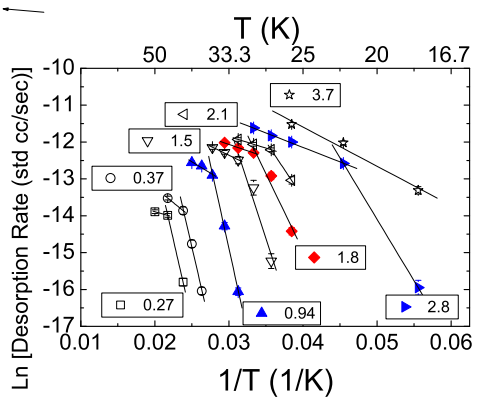

FIG. 8: (color online) Log of desorption rates *vs.* reciprocal temperature plot for the desorption rate isotherm analysis on the SWNT1-2 sample. The coverages where the data points were obtained are shown as the boxed numbers on the graph in terms of 10^{17} atom/mg units. Slopes on this plot are the activation energy for desorption.

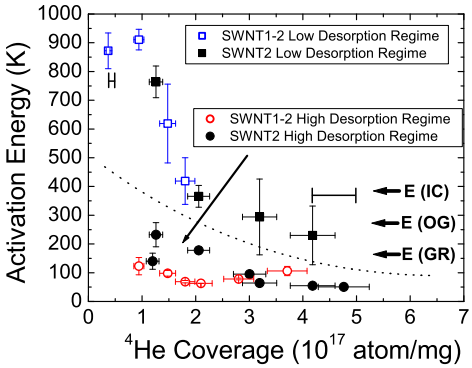

FIG. 9: (color online) Activation energies for desorption from SWNT1-2 and SWNT2 samples. Activation energy obtained from slopes from the high and low desorption rate regimes are shown together. The dotted line in the middle separates the data points from different regimes. An additional error originated from the sample mass uncertainty and is separately indicated by two additional error bars on the plot, shown at high and low coverages. Expected binding energy values on different binding sites on the SWNT bundle (Table I) are also indicated on the plot (arrows).

high-rate desorption occurs.

The high activation energy values from the low desorption rate regime showed ^{4}He binding energy values of OG (∼244 K), IC (∼386 K), and increased beyond IC values at lower coverage (910 K) (Fig. 9). We do not understand why such a high binding energy value was observed from our analysis. Maybe diffusive desorption from porous sites such as IC sites could have affected the analysis of the data or stronger than expected binding sites for ^{4}He might exist on SWNT bundles. Calbi *et al.* predicted such strong binding sites for H_2 at the entrance of IC sites[12] and our observations may imply something similar for ^{4}He. It is also interesting to note that the theoretical calculations by Johnson *et al.* have indicated that the defective IC sites with larger diameter could play a role in CH_4, Ar, Xe, and Ne adsorption on SWNT bundles affecting the measured binding energies[17,42,43].

We compared the desorption activation energies (E_d) we obtained from the low desorption rate regime to the isosteric heat measurement results (q_{st}) from Vilches' group[25] as shown in Fig. 10[54]. Our desorption activation energy values agreed with Vilches' isosteric heat values where the coverages overlap. However, our values continued the trend of increasing energy as the coverage decreased. For the case of non-activated adsorption (without the adsorption barrier energy) the amount of heat released upon adsorption (isosteric heat, q_{st}) and the amount of heat acquired upon desorption (activation energy for desorption, E_d) are supposed to be the same. (^{4}He physisorption to a SWNT bundle is not supposed to be an activated process. However as shown in the next section, we observed about ∼20 K adsorption activation energy on some of the binding sites on our SWNT samples. But this value is less than 10% of the energy values plotted in Fig. 10.) Therefore the agreement (within ∼10 %) of our energy values and Vilches' isosteric heat measurements at the same coverage is expected and our energy values confirm this.

The strong coverage dependence of the desorption activation energy is an indication of a strongly heterogeneous binding surface where there are energetically favored sites so that the adsorbates bind to the strong sites first at low coverage[44].

According to our data, the high binding energies (above 500 K) appeared below about 0.006 std cc/mg coverage that corresponds to 0.025 monolayer (ML) comparing with Vilches previous data[25] which indicated that full ML coverage was about 0.24 std cc/mg. It could be speculated that the small number of defective IC sites with larger diameter in a heterogeneous SWNT bundle are the sites of such high binding energy sites[17,42,43].

B. Dose-Temperature Dependence of ^{4}He Adsorption

The ^{4}He dose temperature was varied to examine the temperature dependence of ^{4}He binding to the single-wall carbon nanotube (SWNT) bundle and to the charcoal samples. For charcoal, the ^{4}He adsorpiton did not depend on the dose temperature, however, for the SWNT sample the ^{4}He adsorption coverage was smaller when dosed at low temperature indicating an energy barrier to access of ^{4}He to some binding sites on the SWNT bundles at low temperature. ^{4}He diffusion coefficient at 15.4 K was found to be 2.9±1.8 nm^2/sec (see Fig. 16) and at 8.5 K found to be close to 0 nm^2/sec (see Fig. 17). We ob-

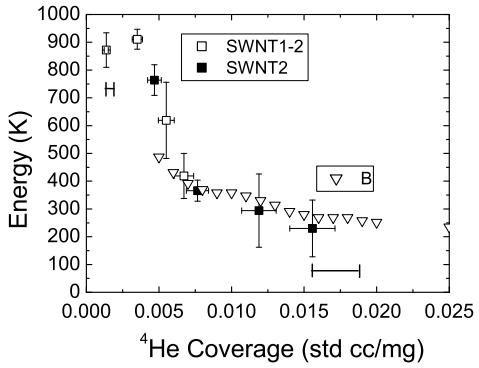

FIG. 10: ^{4}He binding energy dependence on coverage measured on the samples SWNT1-2 and SWNT2 are compared with the results of provided by Vilches and his collaborators[25]. Square points are our results as shown in Fig. 9 but with different units for the x-axis. Only energies obtained from the low desorption rate regime are shown. All three separate measurement results agree with each other where the coverages overlap. Unit conversion: 1 std cc/mg = 2.685×10^{19} atom/mg. Error bars are shown for our results. An additional error originated from the sample mass (20 %) is separately indicated by two additional error bars on the plot, shown at high and low coverages.

tained ^{4}He coverage *vs.* dose-temperature (T_{dose}). When the dose-temperature (T_{dose}) increased, the ^{4}He coverage increased and when T_{dose} was ∼30 K or bigger, then ^{4}He adsorption and desorption was similar to the high-T dose runs (dosed at 275 K). Using an activated diffusion model-fit[45], we obtained the ^{4}He activation energy for adsorption to some binding sites on the SWNT sample to be ∼20 K. We believe that the location of these sites that show activated adsorption behavior at low temperature are the IC sites and the other sites that showed no activation energy are OG sites. And this activated adsorption behavior to IC sites is likely the reason why some of the previous gas adsorption studies (which dose gases at low temperature) did not detect gas adsorption to the IC sites.

We first tested the effect of T_{dose} variation on ^{4}He adsorption for the charcoal sample. High-T dose runs and T_{low}-dose runs were done and the results were compared. For high-T dose runs we put ^{4}He gas into the sample cell at ∼275 K as we did above. For T_{low}-dose runs we added ^{4}He gas at T_{low} and waited 30 min before starting the T_{low} pump-out procedure. For both cases the amount of ^{4}He entered was kept constant at ∼1.4 mmole. We obtained two sets of desorption spectra at two T_{low} values (15.6 K and 16.4 K) as shown in Fig. 11. The desorption spectra from T_{low}-dose runs and high-T dose runs were similar. We found that for the charcoal sample, there was no noticeable difference of ^{4}He adsorption amount at the same T_{low} value between T_{low}-dose runs and high-T dose runs as shown in Fig. 12. This adsorption behavior of the charcoal sample indicates that there is no adsorption energy barrier for ^{4}He on the charcoal sample. This can be easily understood since the adsorption sites on the charcoal are on the surface and so ^{4}He should not have any restriction of access to the binding sites.

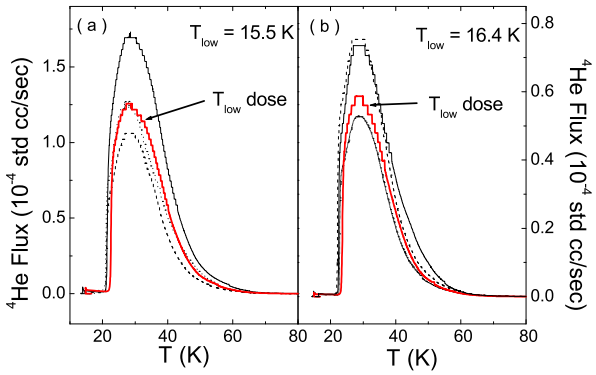

FIG. 11: (color online) ^{4}He desorption spectra comparison of high-T dose and T_{low}-dose runs on a charcoal sample. Spectra from T_{low}-dose runs are plotted with thicker red solid lines and indicated by arrows on both plots. High-T dose run spectra are plotted with black solid, dashed, and dotted lines. Two sets of desorption spectra at two T_{low} values, (a) 15.5±0.2 K and (b) 16.4±0.3 K are shown. There was no noticeable difference between T_{low}-dose runs and high-T dose runs.

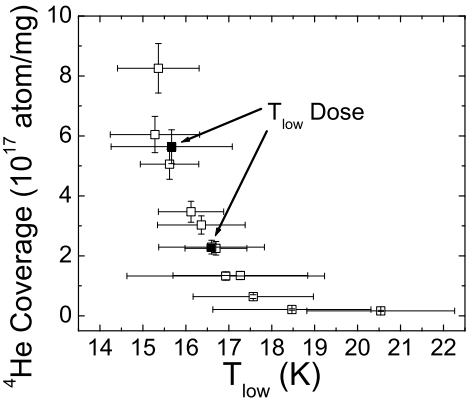

FIG. 12: ^{4}He adsorption comparison of high-T dose and T_{low}-dose runs on a charcoal sample. T_{low}-dose run data points are plotted with filled squares and indicated by arrows. High-T dose run data are plotted with open symbols. There were no differences of ^{4}He adsorption amounts between T_{low}-dose runs and high-T dose runs.

Next we tested the dose temperature dependence of ^{4}He adsorption on the SWNT2 sample. As was done with the charcoal sample, we added ^{4}He gas at 275 K for high-T dose runs and we added ^{4}He gas at T_{low} for T_{low}-

dose runs and waited for 30 minutes before T_{low} pump-out. The amount of ^{4}He added was kept constant at ∼1.4 mmole.

When a similar T_{low} value (15.3 K) as with the charcoal test value was used, we found that for the SWNT sample, the desorption curves were much smaller in T_{low}-dose runs than in high-T dose runs (Fig. 13). Next, we changed the dose-time (the amount time we waited after the gas dose and before starting the T_{low}-pump-out procedure) while keeping the T_{low} value constant and observed the change of the ^{4}He desorption curves. The results showed that the ^{4}He desorption curve size increased as dose-time increased but was still smaller even when a similar dose-time was used in T_{low}-dose runs as in high-T dose runs (Fig. 13). For high-T dose runs, dose-time was 4-5 hours (this included cool-down time of the sample cell). The integrated ^{4}He adsorption amount of T_{low} dose runs at 15.3 K showed that the adsorption amounts of T_{low}-dose runs were about 50% of the amounts of high-T dose runs at similar dose-time. Fig. 14 shows the results.[55]

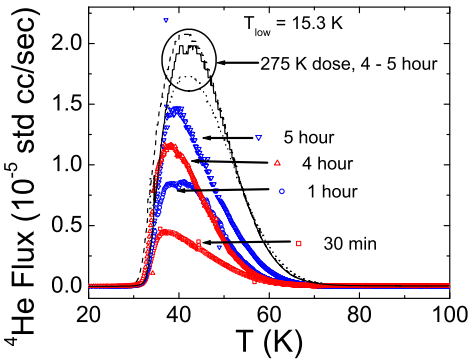

FIG. 13: (color online) ^{4}He desorption spectra with increasing dose-time among T_{low}-dose runs are compared with the spectra from high-T dose runs on the SWNT2 sample. T_{low}-dose run data points are plotted with red symbols. And high-T dose run data are plotted with black lines. Dose times are indicated on the plot. T_{low} for the all runs were kept constant at 15.3±0.3 K. The desorption curve size grew as dose-time increased, however even after we let ^{4}He gas into the sample cell for the same amount of time as the high-T dose runs, the T_{low}-dose runs showed smaller desorption curves than the high-T dose runs.

^{4}He desorption experiments with increasing dose-time in T_{low}-dose runs were done also at a different T_{low} value (8.5 K) on the SWNT1-1 and SWNT2 samples. The amount of ^{4}He added was kept constant at ∼1.9 mmole for SWNT1-1 runs and at ∼1.4 mmole for SWNT2 runs. T_{low}-dose runs showed smaller desorption curves than high-T dose runs. The increase of ^{4}He adsorption as dose-time increased for the 8.5 K T_{low}-dose runs was much slower than for the 15.4 K T_{low}-dose runs as shown in Fig. 15. In fact, an increase of ^{4}He adsorption with dose-time is not present in the data trend. For the SWNT1-1

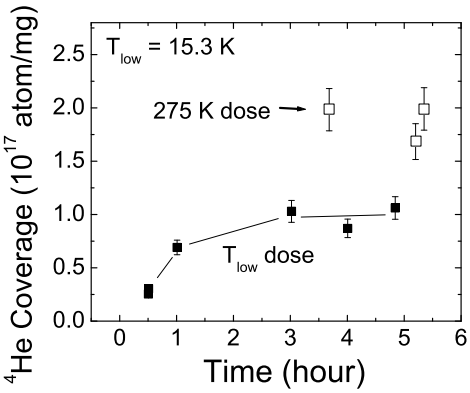

FIG. 14: ^{4}He adsorption amount comparison between T_{low}-dose runs (15.3 K) with varying dose-time and high-T dose runs on SWNT2 sample. T_{low}-dose run data points are plotted with filled squares and high-T dose runs are plotted with open squares. T_{low} for the all runs was kept constant at 15.3±0.3 K. The ^{4}He adsorption amount of the T_{low}-dose runs grew as dose-time increased but only to about 50% of the amounts of high-T dose runs.

runs, the ^{4}He adsorption of T_{low}-dose runs was about 50% of high-T dose runs, for the SWNT2 runs it was about 35%. This difference indicates different adsorption site ratios on these samples per unit mass. (*I.e.* there were more OG sites for the SWNT1-1 sample compared to the SWNT2 sample, if we assume the low-T accessible sites are OG sites and low-T inaccessible sites are IC sites.), which may have been originated from a synthesis-batch-dependant difference between these samples. However, on both samples it was clearly observed that the ^{4}He coverages of the high-T dose runs were 2-3 times bigger than the T_{low}-dose runs.

We think that it is reasonable to interpret the identity of low-T (readily) accessible sites as OG sites and low-T hard-to-access sites as IC sites for two reasons. (1) As the Fig. 13 TPD curves show, the low-T accessible sites had smaller binding energy than the low-T hard-to-access sites (TPD peak temperatures of the T_{low}-dosed curves were lower than the high-T dosed TPD peaks.) (2) OG sites are on the surface of bundles and IC sites are long channels. While the access of ^{4}He to OG sites even at low temperature should be unhindered because they are located on the surface, it is reasonable to expect difficult access to IC sites at low temperature that were accessible through only two openings per channel at the ends of the bundles. It is interesting to note that recent theorecial calculations by Calbi *et al.* have predicted two orders of magnitude longer adsorption time of gases to IC sites compared to OG sites[46]. Their prediction was confirmed by experimental adsorption studies of Ar on open-ended SWNT bundles by Migone *et al.*[47] .

To do a quantitative analysis of the data, we tried applying a random-walk diffusion model[48] to our data. Ac-

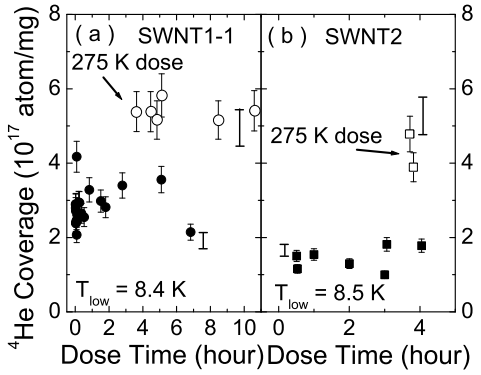

FIG. 15: ^{4}He adsorption amount comparison between T_{low}-dose runs (8.5 K) with varying dose-time and high-T dose runs on SWNT1-1 and SWNT2 samples. (a) shows SWNT1-1 sample results and (b) shows SWNT2 sample results. T_{low}-dose run data points are plotted with filled symbols and high-T dose run data points are plotted with open symbols. The T_{low} value of all the runs was kept constant at 8.4±0.2 K for the SWNT1-1 runs and 8.5±0.1 K for the SWNT2 runs. T_{low}-dose runs had smaller ^{4}He adsorption than high-T dose runs. The maximum coverage on the SWNT1-1 sample was bigger than on the SWNT2 sample, this discrepancy may be due to the SWNT mass uncertainty. 20% error bars due to mass uncertainty are indicated separately on the plot.

cording to this model, an initial packet of particles would diffuse out over time (t) through collisions with the environment similar to a random-walk process, and this packet's mean-square displacement would be described as (in one-dimension),

$$\left\langle x^2 \right\rangle = 2Dt, \tag{1}$$

where $\left\langle x^2 \right\rangle$ is the mean-square displacement and D is the diffusion coefficient. Assuming that the root-mean-square displacement ($\sqrt{\langle x^2 \rangle}$) is proportional to the number of atoms adsorbed (we imagine that ^{4}He atoms adsorbed diffusively into the IC sites.), we plotted the ^{4}He coverage *vs.* the square root of time in Fig. 16. The result looks reasonably linear suggesting that the diffusive adsorption model fits to our data[56]. So we fit the data with a line and obtained the y-intercept (2±15 (10^{15} atom/mg)) and the slope (8 ± 2 (10^{14} atom/mg$\sqrt{\text{sec}}$)) from the fit. The y-intercept number from the fit is the number of ^{4}He atoms that adsorb instantaneously to the SWNT bundle at 15.4 K. We can speculate that the OG sites would have instantaneous access for the ^{4}He atoms and the IC sites have slow diffusive access for the ^{4}He atoms due to the IC sites' tiny size and possible restrictions by adsorption barriers induced by defect sites on SWNTs. A recent calculation by Gordillo *et al.* proposed such a scenario for ^{4}He adsorption to IC sites[14]. Also, Calbi *et al.* have predicted much slower adsorption of gases to IC sites due to diffusive adsorption process[46]. So we interpret the y-intercept value as the number of atoms adsorbed onto OG sites[57].

Using some further assumptions (the mean square displacement divided by the adsorbate distance is the number of adsorbates in the diffusion channel (IC sites)), we obtained the diffusion coefficient from the slope as well. The number of atoms diffusively adsorbed in the IC sites (N_{IC}) may be written as:

$$N_{IC} = N_{total} - N_{OG} = \frac{\sqrt{2D}}{a_{He}} N_{CH} \sqrt{t}, \tag{2}$$

where N_{OG} is the number of ^{4}He atoms on the OG sites, a_{He} is the distance between ^{4}He atoms in the IC sites (= 0.3 nm), and N_{CH} is the number of channels that ^{4}He atoms diffuse within (= 9.6× 10^{13} channel/mg, obtained from the sample model discussed elsewhere[49]). The obtained diffusion coefficient was 2.9± 1.8 nm^2/sec.[58] The small size of the diffusion coefficient is different from some of the theoretical predictions on gas adsortption to SWNT bundles: in ID sites, a molecular simulation done by D. Sholl and colleagues has indicated that on the ID sites of SWNTs for H_2 and CH_4 the diffusion coefficient (∼1 cm^2/sec) will be much higher than other silicate micro porous materials due to the surface smoothness of the SWNTs[45]. However other predictions[14,50] are in line with our findings: the possible small mobility of the ^{4}He atoms inside of the IC sites might be due to the collaborations of the corrugated potentials of the adjoining SWNT surfaces in the IC sites[50] or due to the potential barrier due to defect sites on the SWNT surface[14].

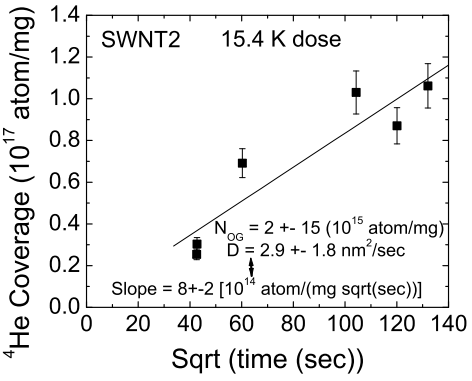

FIG. 16: ^{4}He coverage *vs.* square root of dose-time of 15.4 K dose runs on SWNT2. A linear fit is shown. The slope and the y-intercept value (N_{OG}) are included on the graph. The diffusion coefficient (D) calculated from the slope is indicated also.

The same random-walk diffusion model fitting was applied to our data obtained at 8.5 K as plotted in Fig. 17. This time the data yielded much flatter fit indicating the diffusion coefficient at this temperature was ∼0.01 nm^2/sec. (But, see the caption to Fig. 17.) The N_{OG}

obtained was 2.67 ± 0.17 (10^{17} atom/mg) from SWNT1-1 and 1.29 ± 0.30 (10^{17} atom/mg) from SWNT2. The N_{OG} value of the SWNT2 sample obtained from the 8.5 K runs (1.3×10^{17} atom/mg) disagreed somewhat with the N_{OG} value from the 15.4 K runs (2×10^{15} atom/mg) indicating that the confidence in the fit should be low.

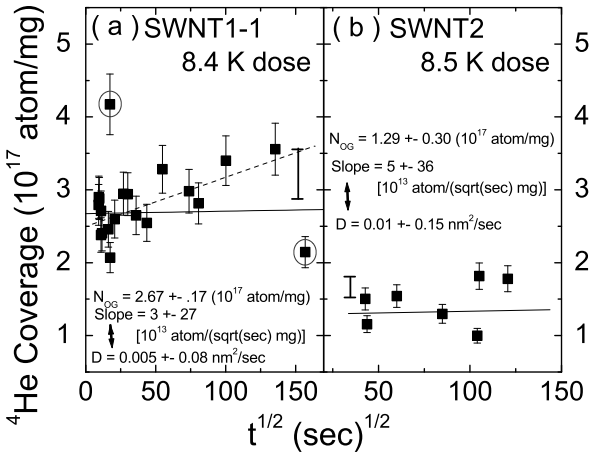

FIG. 17: ^{4}He coverage *vs.* square root of dose-time of 8.5 K dose runs from SWNT1-1 and SWNT2. Linear fits are also shown. The slopes and the y-intercept values (N_{OG}) are included on the graph. The diffusion coefficients (D) calculated from the slope values are indicated also. An additional error originated from the sample mass uncertainty (20%) are indicated separately by additional error bars. A dashed line on (a) indicates an alternate plot to the data if the two circled data points are excluded. This alternate fit resulted N_{OG} = 2.51±0.09 (10^{17}), and slope = 7.4±1.8 (10^{14}): D = 2.7±0.2. (Same units as indicated in the figure.) We did not find any valid reason to exclude the circled data points, but they are well off the trend suggested by the rest of the data.

In order to check the ^{4}He adsorption change with a dose-temperature change, we tried changing T_{dose} while keeping T_{low} at 8.5 K. The experimental procedure used was: for high-T dose runs we put ^{4}He gas into the SC immediately after the warm-up sequence as we did above, and for low-T dose runs we cooled down to a preset temperature (T_{dose}) first and then charged the SC with ^{4}He gas and waited for 30 minutes before cooling down to T_{low}. The T_{low} value for each sample run was kept constant. At T_{low}, the T_{low}-pump-out procedure was done followed by the rest of the experimental procedures mentioned earlier. For SWNT1-1 T_{low} = 8.4 K, and for SWNT2 T_{low} = 8.5 K and the amount of ^{4}He added was also kept constant (∼1.9 mmole for SWNT1-1, ∼1.4 mmole for SWNT2). Fig. 18 shows the desorption curves for ^{4}He obtained from the SWNT2 sample. With T_{dose} at 8.5 K, the desorption curve is much smaller and the peak temperature was lower than for the high-T dosed desorption curve. As T_{dose} increased, the desorption curves grew in size and also the peak temperature shifted toward higher temperature, and with T_{dose} at 46.5 K the desorption curve looked similar to high-T dose curve indicating the adsorption of ^{4}He at this dose temperature is the same as for the 275 K dose case. The same measurements on the SWNT1-1 sample showed a similar trend.

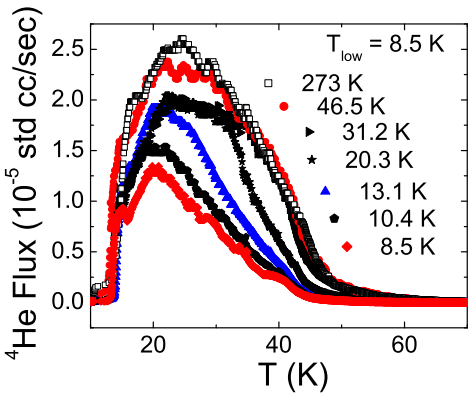

FIG. 18: (color online) ^{4}He desorption spectra with increasing dose-temperatures from the SWNT2 sample. T_{low} for all the runs was 8.5±0.4 K. Low-T dose run data points are plotted with filled symbols and high-T dose run data are plotted with open symbols. T_{dose} values are indicated on the plot. The desorption curve size grew as T_{dose} increased and became similar in size as for the high-T dose run: The T_{dose} = 46.5 K curve indicates this.

We integrated the ^{4}He desorption curves to obtain the ^{4}He adsorption *vs.* T_{dose} data as shown in Fig. 19. The ^{4}He adsorption amount increased as T_{dose} increased from the minimum value at 8.4 K and when T_{dose} was about 30 K or larger then there were no big differences in the ^{4}He adsorption amounts between low-T dose runs and high-T dose runs. There is about 20-50% more adsorption on the SWNT1-1 sample than on the SWNT2 sample. This difference may be partly due to the sample mass uncertainty (20%) and also may be due to a difference in the adsorption sites ratio (N_{OG}/N_{IC}) as mentioned earlier.

We tried to fit our ^{4}He adsorption amount *vs.* T_{dose} to the activated diffusion model[45], where the diffusion of the molecules on the surface is explained by an activated process. This kind of diffusion can happen when the pore sizes are so small that the surface corrugation affects the molecule movement within the pores. For the activated diffusion process, the temperature dependence of the diffusion coefficient (D_a) is described as,

$$D_a = D_0 \exp(-E_a/T) \qquad (3)$$

where D_0 is a prefactor and E_a is the activation energy of the diffusion. As shown in Eqn. 2, $N_{IC}^2 \propto D$ when t is constant. Therefore $\ln N_{IC}^2$ = -E_a/T + constant. Fig. 20 is a plot of our data modeled with the activated diffusion process. From the slope of the fitted line, we obtained the activation energy of diffusion (E_a) to be 14 ± 7 K on

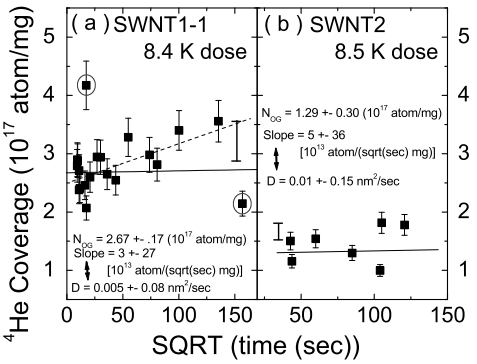

FIG. 19: ^{4}He coverage *vs.* dose-temperature on the SWNT1-1 and SWNT2 samples. For SWNT1-1, T_{low} = 8.4±0.1 K, and for SWNT2, T_{low} = 8.5±0.4 K. Additional error originated from the sample mass uncertainty (20%) are indicated separately by additional error bars. We observed that when T_{dose} is about 30 K or higher, the ^{4}He adsorption was as large as for the high-T dose runs. Note that there is a break in the T_{dose}-axis scale.

SWNT1-1 sample data and 25 ± 10 K on SWNT2 sample data.

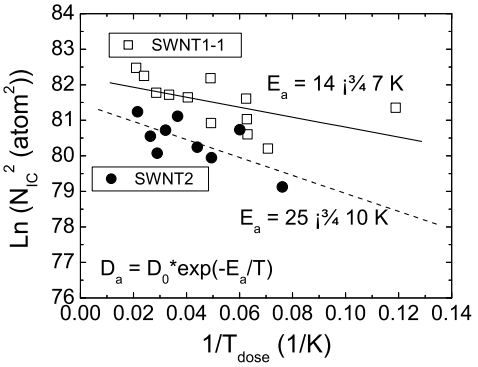

FIG. 20: log $N_{IC}{}^2$ *vs.* $1/T_{dose}$ data from SWNT1-1 and SWNT2 samples. Using the activated diffusion model, we fit the data and obtained ∼20 K for the activation energy for diffusion. This model's equation for diffusion coefficient is indicated and also individual sample fit results are indicated on the plot. Note that we did not normalize the data by sample mass here.

Our findings about the restricted access of ^{4}He to some of the sites in the SWNT bundle might explain why IC adsorption of ^{4}He was not observed in experiments reported so far[19,21] despite theoretical predictions that it should happen[10,11]. These experimental studies exposed SWNT samples at low temperature and at such low temperature IC adsorption of ^{4}He was likely severely restricted as we observed here.

Further, our finding may explain why there are two contradicting observations on the specific heat of ^{4}He on SWNT bundles. Lasjaunias *et al.* showed that one-dimensional specific heat behavior was observed[22], while Wilson and Vilches reported that no such one-dimensional behavior was observed[25]. Lasjaunias dosed ^{4}He at 77 K which is a high enough temperature for ^{4}He adsorption to all the allowed binding sites on SWNT, but Wilson carried out studies between 1.5 K and 6 K which, according to our findings, would be too low a temperature for ^{4}He access to the IC sites.

C. Competitive Adsorption of Binary Gas Mixtures

We investigated ^{4}He-H_2, ^{4}He-Xe, H_2-Xe, and ^{3}He-^{4}He competitive adsorption to a SWNT bundle sample. First, we observed that H_2 suppressed ^{4}He adsorption to the background level when H_2 and ^{4}He were simultaneously dosed in equal amounts at 275 K. However, when ^{4}He was first added at 275 K and H_2 was added after the sample was cooled down to 19 K, the ^{4}He adsorption was not completely displaced by H_2, as is the case when both gases are dosed at 275 K. Second, we observed that a small amount (∼5%) of Xe co-dosed with ^{4}He or H_2 at 275 K suppressed ^{4}He or H_2 adsorption completely. Third, we observed that an equal amount of ^{4}He and ^{3}He co-dosed at 275 K yielded 8.4 times more ^{4}He adsorption than ^{3}He indicating a strong quantum sieving effect[6] on the SWNT sample.

^{4}He and H_2 mixture adsorption to the SWNT2 sample was measured. As we have reported previously[28], when dosed in equal amounts at 275 K, H_2 blocked ^{4}He adsorption to the SWNT bundle completely (Fig. 21, a1 and a2). Next we tried changing the H_2 dose temperature to 19 K. The procedure for this measurement was as follows. After the ^{4}He dose at 275 K, the sample cell temperature was lowered to 19 K and then H_2 was added to the sample cell for 30 minutes. And the T_{low}-pump-out procedure was done followed by the rest of the procedures mentioned above (T_{min}-cool-down was not done). We found that H_2 could not suppress ^{4}He adsorption to the SWNT sample when ^{4}He was dosed first at 275 K and H_2 was later dosed at 19 K (Fig. 21, b1 and b2). This means that the sites where ^{4}He was adsorbed were not accessible to H_2 at 19 K within 30 minutes time. The ^{4}He adsorption amount was similar to the ^{4}He adsorption amount for the runs where ^{4}He was dosed alone. H_2 also has some limited access to some of the binding sites on the SWNT sample. The H_2 desorption peak was smaller when dosed at 19 K than 273 K and its size was about the same size whether ^{4}He was present or not indicating the smaller H_2 peak was not due to ^{4}He (Fig. 21, b1). Total dosage of gases to the sample cell for each run was fixed at ∼1.4 mmole. Mixture doses were done at a 50-50 ratio (*i.e.* each gas 0.7 mmole). Mixture dose runs were repeated more than once and they reproduced[59].

Here we also interpret our observation of the limited

access of H_2 at low temperature to some binding sites on the SWNT bundle as due to limited access to IC sites on the SWNT bundle. Also for high-T ^{4}He and low-T H_2 results, we interpret that when dosed at high-T, ^{4}He accessed the IC sites and these were protected from H_2 when H_2 was dosed at 19 K.

Theoretical calculations by Calbi *et al.* have predicted the possible existence of trap sites at the entrance of IC sites that inhibit H_2 adsorption to IC at low temperature[12,46], and also much longer adsorption time on IC sites compared to OG sites[46]. Also the same mechanism discussed above by Gordillo[14] might explain the limited access of H_2 to IC at low temperature.

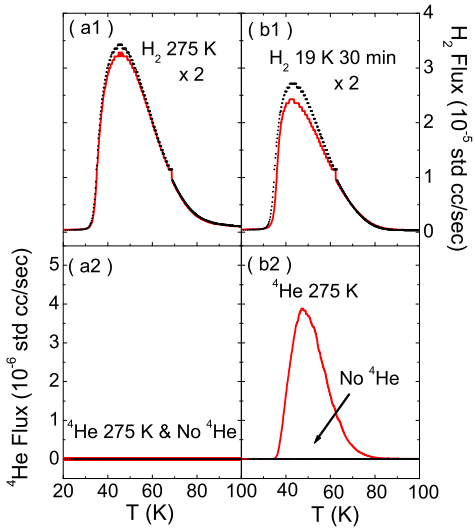

FIG. 21: (color online) ^{4}He and H_2 desorption spectra comparisons of high-T dose and T_{low}-dose runs on the SWNT2 sample. (a1) and (a2) show two sets of desorption spectra of H_2 and ^{4}He. Red solid lines show when both H_2 and ^{4}He were dosed at 275 K. Black dotted lines show when H_2 was dosed alone at 275 K. The presence of H_2 completely suppressed ^{4}He adsorption and H_2 adsorption was not affected by the presence of ^{4}He. (b1) and (b2) each show two sets of spectra. Red solid lines show the spectra when we add ^{4}He at 275 K, cooled the sample cell to 19 K and then added H_2 to the SC for 30 minutes. Black dotted lines show the spectra when we dosed H_2 alone at 19 K for 30 minutes. We observed a prominent ^{4}He desorption peak in the first set (b2, red line). 19 k dosed H_2 desoption peaks (b1) were smaller than 275 K dosed peaks (a1). H_2 desorption peaks in (b1) were approximately the same size whether ^{4}He was present or not indicating that the smaller H_2 peak was not due to ^{4}He. T_{low} for all the runs was 18.0±0.3 K.

After the H_2 and ^{4}He codesorption experiments we checked the cleanliness of the SWNT2 sample by comparing the ^{4}He adsorption amount to the previously established T_{low} scan for ^{4}He coverage on the SWNT2 sample. The ^{4}He coverage was about the same as the previous ^{4}He runs, indicating the sample was clean after the H_2 codesorption runs.

Next we conducted Xe co-dose experiments with ^{4}He or H_2 on the SWNT2 sample. For the measurements, we put ∼5% Xe in the mixture gas dose at 275 K and procedures mentioned above were followed[60]. Only ^{4}He or H_2 desorption was measured since our mass spectrometer could not detect Xe. The spectra obtained in these tests are plotted in Fig. 22. When Xe was co-dosed, both H_2 and ^{4}He adsorption suppressed almost to the background level. Xe co-dose runs for both gases were reproduced. T_{low} for these measurements was 18.2 K.

According to theoretical predictions[10], Xe's binding energy on OG sites is stronger than H_2 and ^{4}He, and Xe is too big to enter IC sites. So our observations could be interpreted to indicate that only OG sites are available for adsorption for H_2 and ^{4}He. However, if IC entrances were blocked by Xe, then it would also prevent H_2 and ^{4}He adsorption to IC sites.

An additional experiment could have been that if H_2 and ^{4}He entered first at 275 K and Xe dosed at a low enough temperature then H_2 and ^{4}He adsorption to the SWNT binding sites already happened. But, this experiment could not be carried out in our apparatus because Xe has a very high boiling point (166 K at 1 atm) making it difficult to transfer into the sample cell at ∼10 K temperature.

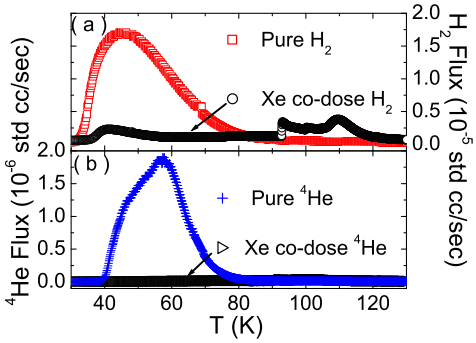

FIG. 22: (color online) ^{4}He and H_2 desorption spectra comparisons between pure gas dose runs and Xe co-dose runs. (a) show H_2 desorption comparisons, and (b) show ^{4}He desorption comparisons. When Xe was co-dosed, both H_2 and ^{4}He adsorptions were suppressed almost to the background level. The small peaks near 100 K in (a) may be due to freeing of Xe capsulated H_2 from IC sites when Xe migrated away from the entrance sites of IC. T_{low} for these measurements were 18.2 K. The amounts dosed (at 275 K) for co-dose runs were (a) H_2 = 1.4 mmole and Xe = 0.1 mmole, (b) ^{4}He = 1.5 mmole and Xe = .06 mmole. For pure gas dose runs, the amount dosed was 1.4 mmole.

We also checked the sample cleanliness of the SWNT2 sample after the Xe codose experiments by measuring the ^{4}He adsorption amount and comparing them to the previously measured T_{low}-scan run results. After Xe exposure to SWNT sample, we observed that the ^{4}He adsoption decreased to about 58% of a clean sample level indicating

that either Xe desorption was not complete by pumping up to 275 K or the SWNT2 sample was partially contaminated at this stage of the experiment.

Next we tried ^{4}He and ^{3}He coadsorption to the SWNT2 sample. These results were reported previously[30] but we include them in this paper for comparison and completeness. When both species entered the sample cell in 50-50 mixture, ^{4}He adsorption was 8.4 times more than ^{3}He adsorption (Fig. 23). We reproduced this result. This preferential binding of ^{4}He isotope over ^{3}He is compatible with the predictions of strong quantum sieving effects on the SWNT binding sites[6].

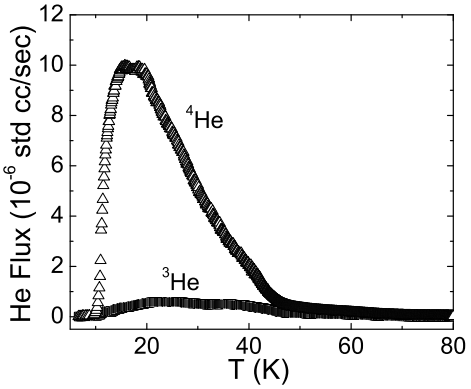

FIG. 23: He isotopic desorption spectra comparison when co-dosed. T_{low} was 6.8 K. The amount dosed at 273 K for each gas was ∼0.7 mmole. We observed that when equal amounts of ^{4}He and ^{3}He were dosed to the SWNT sample, the ^{4}He adsorption was 8.4 times more than the ^{3}He adsorption.

V. CONCLUSION

The temperature-programmed desorption studies of ^{4}He onto SWNT bundles have confirmed the existence of strong binding energy sites on SWNT bundles. The ^{4}He coverage-dependent binding energy on SWNT bundles was obtained and compared with the binding energy on a charcoal sample. The activation energy of ^{4}He to some binding sites on SWNT bundles was obtained. We argued that the identity of these sites with adsorption activation energy are IC sites. The ^{4}He-H_2 codesorption studies confirmed that H_2 binds preferentially on SWNT bundles compared to ^{4}He. However low temperature H_2 adsorption to the SWNT sample with pre-adsorbed ^{4}He indicated that H_2 also has an access-barrier to some of the sites on SWNT bundles. The ^{4}He-Xe and the H_2-Xe codesorption studies showed that a small amount of Xe blocks most of the ^{4}He and H_2 access to SWNT bundles. The ^{4}He-^{3}He codesorption run showed the quantum sieving effect among helium isotopes on the SWNT bundles.

Acknowledgments

We thank T.W. Ebbesen for contributions to our early work. We also thank M. Tuominen for the loan of equipment. We have benefited from a series of very helpful discussions with O.E. Vilches, M.M. Calbi and M. Cole. Some equipment supplied by NSF DMR 98-19122 for other studies was used for our measurements. Acknowledgement is made to the donors of the Petroleum Research Fund, administered by the ACS, and Research Trust Funds from the University of Massachusetts Amherst for support of this research. We also benefitted from access to the facilities of the University MRSEC supported by the NSF.

* Current Address: Research Institute for Solar and Sustainable Energies (RISE), Gwangju 500-712, Rep. of Korea
† hallock@physics.umass.edu

[1] M. Dresselhaus, G. Dresselhaus, and P. Eklund, *Science of Fullerenes and Carbon Nanotubes* (Academic Press, Boston, 1996).
[2] P. Ajayan and T. Ebbesen, Rep. Prog. Phys. **60**, 1025 (1997).
[3] A. Thess, R. Lee, P. Nikolaev, H. Dai, P. Petit, J. Robert, C. Xu, Y. Lee, S. Kim, A. Rinzler, et al., Science **273**, 483 (1996).
[4] A. Dillon, K. Jones, T. Bekkedahl, C. Kiang, D. Bethune, and M. Heben, Nature **386**, 377 (1997).
[5] P. Chen, X. Wu, J. Lin, and K. Tan, Science **285**, 91 (1999).
[6] Q. Wang, S. Challa, D. Sholl, and J. Johnson, Phys. Rev. Lett. **82**, 956 (1999).
[7] D. Goulding, J.-P. Hansen, and S. Melchionna, Phys. Rev. Lett. **85**, 1132 (2000).
[8] A. Fedorov, P. Avramov, S. Ovchinnikov, and G. Kresse, Europhys. Lett. **63**, 254 (2003).
[9] M. Cole, V. Crespi, G. Stan, C. Ebner, J. Hartman, S. Moroni, and M. Boninsegni, Phys. Rev. Lett. **84**, 3883 (2000).
[10] G. Stan, M. Bojan, S. Curtarolo, S. Gatica, and M. Cole, Phys. Rev. B **62**, 2173 (2000).
[11] M. Calbi, F. Toigo, and M. Cole, Phys. Rev. Lett. **86**, 5062 (2001).
[12] M. Calbi and J. Riccardo, Phys. Rev. Lett. **94**, 246103 (2005).
[13] M. Gordillo, J. Boronat, and J. Casulleras, Phys. Rev. Lett. **85**, 2348 (2000).
[14] M. Gordillo, Phys. Rev. Lett. **96**, 216102 (2006).
[15] S. Weber, S. Talapatra, C. Journet, A. Zambano, and A. Migone, Phys. Rev. B **61**, 13150 (2000).
[16] M. Muris, N. Dufau, M. Bienfait, N. Dupont-Pavlovsky, Y. Grillet, and J. Palmari, Langmuir **16**, 7019 (2000).
[17] W. Shi and J. Johnson, Phys. Rev. Lett. **91**, 015504 (2003).
[18] S. Ramachandran, T. Wilson, D. Vandervelde, D. Holmes, and O. Vilches, J. Low Temp. Phys. **134**, 115 (2004).
[19] S. Talapatra, A. Zambano, S. Weber, and A. Migone, Phys. Rev. Lett. **85**, 138 (2000).
[20] S. Talapatra, V. Krungleviciute, and A. Migone, Phys. Rev. Lett. **89**, 246106 (2002).
[21] J. Pearce, M. Adams, O. Vilches, M. Johnson, and H. Glyde, Phys. Rev. Lett. **95**, 185302 (2005).
[22] J. Lasjaunias, K. Biljaković, J. Sauvajol, and P. Monceau, Phys. Rev. Lett. **91**, 025901 (2003).
[23] T. Wilson, A. Tyburski, M. DePies, O. Vilches, D. Becquet, and M. Bienfait, J. Low Temp. Phys. **126**, 403 (2002).
[24] T. Wilson and O. Vilches, Physica B **329**, 278 (2003).
[25] T. Wilson and O. Vilches, Low Temp. Phys. **29**, 732 (2003).
[26] W. Teizer, R. Hallock, E. Dujardin, and T. Ebbesen, Phys. Rev. Lett., **82**, 5305 (1999); Ibid, **84**, 1844 (2000).
[27] Y. Kahng, R. Hallock, E. Dujardin, and T. Ebbesen, J. Low Temp. Phys. **126**, 223 (2002).
[28] Y. Kahng, R. Hallock, and E. Dujardin, Physica B **329 (1)**, 280 (2003).
[29] R. Hallock and Y. Kahng, J. Low Temp. Phys. **134**, 21 (2004).
[30] Y. Kahng, R. Hallock, and M. Calbi, J. Low Temp. Phys. **138**, 217 (2005).
[31] M. Bienfait, P. Zeppenfeld, N. Dupont-Pavlovsky, J.-P. Palmari, M. Johnson, T. Wilson, M. DePies, and O. Vilches, Phys. Rev. Lett. **91**, 035503 (2003).
[32] W. Teizer, Ph.D. thesis, University of Massachusetts at Amherst (1998).
[33] T. Guo, P. Nikolaev, A. Thess, D. Colbert, and R. Smalley, Chem. Phys. Lett. **243**, 49 (1995).
[34] E. Dujardin, T. Ebbesen, A. Krishnan, and M. Treacy, Adv. Mater. **10**, 1472 (1998).
[35] A. Kuznetsova, J. Yates, Jr., J. Liu, and R. Smalley, J. Chem. Phys. **112**, 9590 (2000).
[36] R. Cvetanović and Y. Amenomiya, Adv. Catal. **17**, 103 (1967).
[37] C. Kittel and H. Kroemer, *Thermal Physics* (W.H. Freeman, New York, 1980).
[38] J. Falconer and J. Schwarz, Catal. Rev.-Sci. Eng. **25** (1983).
[39] M. Jäckel and F. Fietzke, Vacuum **44**, 421 (1993).
[40] W. Press, S. Teukolsky, W. Vetterling, and B. Flannery, *Numerical Recipes 2nd. ed.* (Cambridge University Press, New York, 1992).
[41] S. Talapatra and A. D. Migone, Phys. Rev. B **65**, 045416 (2002).
[42] M. LaBrosse, W. Shi, and J. Johnson, Langmuir **24**, 9430 (2008).
[43] M. LaBrosse and J. Johnson, J. of Phys. Chem. C **114**, 7602 (2010).
[44] J. Dash, *Films on Solid surfaces* (Academic Press, New York, 1975).
[45] A. Skoulidas, D. Ackerman, J. Johnson, and D. Sholl, Phys. Rev. Lett. **89**, 185901 (2002).
[46] J. Burde and M. Calbi, J. of Phys. Chem. C **111**, 5057 (2007).
[47] D. Rawat, M. Calbi, and A. Migone, J. of Phys. Chem. C **111**, 12980 (2007).
[48] F. Reif, *Fundamentals of statistical and thermal physics* (McGraw-Hill, Inc., New York, 1965).
[49] Y. Kahng, Ph.D. thesis, University of Massachusetts at Amherst (2005).
[50] M. Boninsegni, S. Lee, and V. Crespi, Phys. Rev. Lett. **86**, 3360 (2001).
[51] G. Stan and M. Cole, Surface Science **395**, 280 (1998).
[52] K. Hahn, J. Kärger, and V. Kukla, Phys. Rev. Lett. **76**, 2762 (1996).
[53] The main effect of this process is to desorb water from the sample surface.
[54] The binding energy (E_b) is supposed to be different from the isosteric heat (q_{st}) (= the activation energy for desorption (K) less the activation energy for adsorption) by a factor of $\sim T$ (K) (or more specifically, for the low temperature and low coverage regime; $q_{st} \simeq E_b + (1/2)T$ for the system of classical 2D (and 1D) adsorbates; and $q_{st} \simeq E_b + 2T$ for the system of 1D quantum adsorbates[51]). Our measurements and Vilches' measurements were done at the temperatures of ∼10 Ks, so for the activation energy values reported in this graph, the difference between the activation energy and the binding energy should be at most ∼10%.
[55] Such ^{4}He TPD spectra comparison of the T_{low}-dose runs and the high-T dose runs was repeated on another sample,

SWNT1-2. SWNT1-2 sample's low-T adsorption behavior was different from the SWNT2 sample. With T_{low} at 15.2 K. Runs with 30 min and 1.5 hour dose-time had flat ^{4}He desorption curves and a run with 3.5 hour dose-time had a distinctive desorption peak, the size of which was smaller than high-T dose run's peaks. I.e., there was much less ^{4}He adsorptioni in T_{low}-dose runs on the SWNT1-2 sample than on the SWNT2. This difference may be because the SWNT1-2 sample had a very small number of binding sites available for adsorption at low temperatures. TEM study conducted on this sample later showed more impurities on this sample which may have been introduced during handling of the sample for baking in our lab. Lack of low-T accessible adsorption sites might be due to impurities covering the surfaces of the bundles.

[56] Such square root of time dependence of mean square displacement of molecules in diffusion has been reported by K. Hahn *et al.*[52]. Using a pulsed field gradient NMR, they monitored CF_4 (0.47 nm diameter) diffusion in 0.73 nm diameter one-dimensional channels of a zeolite sample at 180 K.

[57] However, according to the Calbi *et al.* calculation[46], even the adsorption to OG sites is not an instantaneous process as we assume here.

[58] If the N_{CH} number were incorrect, then this would affect the diffusion coefficient. If, for example, some of the IC were blocked by impurities and therefore only few of ICs were open, then D value would be calculated to be lower than the actual value. If real N_{CH} was 100 times smaller than real D would be 10,000 times bigger.

[59] For dual gas monitoring we used two leak detectors to monitor desorption the flux simultaneously; each leak detector monitored one gas. So the desorption flux reported in these plots are roughly one-half of the total flux.

[60] Since Xe's boiling point was 166 K (at 1 atm), we could not use a liquid nitrogen trap on the line though which we admitted Xe. We used only small amount of Xe in the mixture in order to avoid Xe condensation in the pump-out liquid nitrogen trap during the flushing and filling cleaning of the gas lines.